Available online at www.sciencedirect.com
SCIENCE DIRECT®
Journal of Sound and Vibration 281 (2005) 235–259
JOURNAL OF SOUND AND VIBRATION
www.elsevier.com/locate/jsvi

Free vibration analysis of isotropic rectangular plates using a high-order triangular finite element with shear

Mihir Chandra Manna

Bengal Engineering College (Deemed University), P.O. Botanic Garden, Howrah 711 103, West Bengal, India

Received 24 July 2002; accepted 15 January 2004
Available online 22 September 2004

Abstract

In this paper, free vibration analysis of isotropic rectangular plates with different thickness ratios, different boundary conditions and different aspect ratios has been investigated using a high-order triangular element. The first-order shear deformation theory (FOSDT) is used to include the effect of transverse shear deformation. The element has 18 nodes on the sides and six internal nodes. The geometry of the element is expressed by three linear shape functions of area coordinates. The formulation is displacement type and the use of area coordinates makes the shape functions for field variables to be expressed explicitly. No numerical integration is required to get the element stiffness and consistent mass matrices. The element has 51 degrees of freedom, which can be reduced to 39 degrees of freedom by Guyan reduction, mass condensation, or eigenvalue economization scheme for the degrees of freedom associated with the internal nodes. Rotary inertia has been included in the consistent mass matrix. Numerical examples are presented to show the accuracy and convergence characteristics of the element.

1. Introduction

Structures of plates and shells have wide applications in ships, aircrafts, bridges, etc. A thorough study of their dynamic behavior and characteristics is essential to assess and use the full potentials of plates and shells. The finite element method has been proved to be a more versatile

E-mail address: mcmbecdu@lycos.com (M.C. Manna).

0022-460X/$ - see front matter © 2004 Elsevier Ltd. All rights reserved.
doi:10.1016/j.jsv.2004.01.015

tool in engineering fields [1,2]. Plate bending is one of the first problems where the application of finite element was done in the early 60s. A number of difficulties were faced when Kirchoff's hypothesis was applied to analyze bending as well as free vibration of thin plates. These are mostly associated with the satisfaction of normal slope continuity on the interfaces between various elements. The above-mentioned slope continuity problem has been eliminated by applying the well-known Reissner–Mindlin's hypothesis for thick plates. In Reissner–Mindlin's hypothesis the transverse displacement (w) and rotations of normal (θ_x and θ_y) are expressed as independent field variables. A large number of published works on plate vibration are available as may be seen by inspection of the excellent review articles by Leissa [3–9] and Liew et al. [10] and other comprehensive works by Yamada and Irie [11], Leissa [12], Liew et al. [13], Dickinson and Blasio [14], Lim et al. [15], Cheung and Zhou [16] and Zhou et al. [17]. Also, a large number of triangular and quadrilateral finite elements were developed for analysis of thin as well as thick plates among which isoparametric elements became more popular [18]. Shear locking, stress extrapolation and spurious modes are some problems faced by these elements instead of having high elegacy. To avoid the above-mentioned problems a number of thick plate bending elements have been proposed by Petrolito [19], Yuan and Miller [20], Sengupta [21], Batoz and Katili [22] and Zhongnian [23] and others. Sheikh et al. [24] have used mass lumping schemes to form the mass matrix having zero mass and zero rotary inertia for the internal nodes of the element to facilitate the condensation process without considering the off-diagonal terms of the mass matrix. The results using the Guyan reduction scheme [25] by the element proposed by Sheikh et al. [24] have not been reported in their work.

The present paper utilizes a triangular element with 18 nodes equidistantly placed on the sides and six nodes internal to it. The element has three degrees of freedom (w, θ_x, θ_y) at the three nodes on the vertices (nodes 1, 7 and 13), at six side nodes nearer to midside nodes (nodes 3,5,9,11,15 and 17) and at three internal nodes (nodes 22–24), two degrees of freedom (θ_x, θ_y) at midpoint nodes (nodes 4, 10 and 16) and a single degree of freedom (w) at the remaining nodes (nodes 2, 6, 8, 12, 14 and 18–21). The element geometry is described by linear shape functions of area coordinates including corner nodes only. In the proposed element the transverse displacement field (w) and both θ_x and θ_y are expressed by a fifth-order polynomial and a fourth-order polynomial, respectively. The nodes are placed on the sides and inside the proposed element such that the mass and rotary inertia for the internal nodes are negligible and the well-known Guyan reduction scheme [25] for the mass condensation is efficiently utilized to get highly accurate natural frequencies of rectangular plates under all 21 boundary conditions involving all possible combinations of clamped, simply supported and free edges.

2. Finite element formulation

The formulation is based on the Reissner–Mindlin plate theory. In this theory it is assumed that the transverse deflection of the plate is small compared to the plate thickness and the normals to the plate midsurface, which is taken as the reference plane, remain straight but may not remain normal to the deformed midsurface. A 24 node triangular element is used to develop the finite element analysis procedure. The element is shown in Fig. 1.

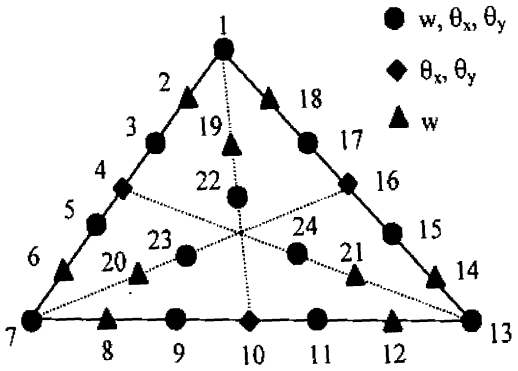

Fig. 1. Present element.

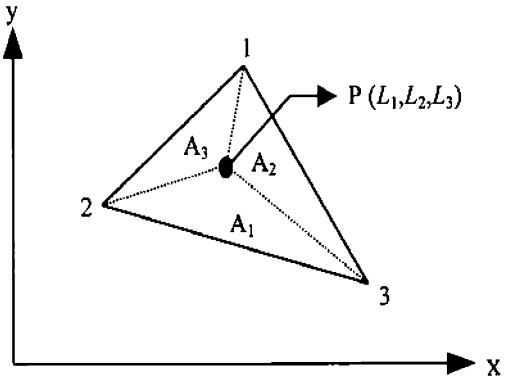

Fig. 2. Area coordinates.

The element has three degrees of freedom (w, θ_x, θ_y) at nodes 1,3,5,7,9,11,13,15,17 and 22–24, two degrees of freedom (θ_x, θ_y) at nodes 4,10 and 16 and a single degree of freedom (w) at nodes 2,6,8,12,14 and 18–21. The area coordinates (L_1, L_2, L_3) of the nodes are $(1,0,0), (\frac{5}{6}, \frac{1}{6}, 0), (\frac{2}{3}, \frac{1}{3}, 0), (\frac{1}{2}, \frac{1}{2}, 0), (\frac{1}{3}, \frac{2}{3}, 0), \quad (\frac{1}{6}, \frac{5}{6}, 0), \ (0,1,0), (0, \frac{5}{6}, \frac{1}{6}), (0, \frac{2}{3}, \frac{1}{3}), \ (0, \frac{1}{3}, \quad \frac{2}{3}), (0, \frac{1}{6}, \frac{5}{6}), \ (0,0,1), \ (\frac{1}{6}, 0, \frac{5}{6}), (\frac{1}{3}, 0, \frac{2}{3}), \ (\frac{2}{3}, 0, \frac{1}{3}), \ (\frac{1}{2}, 0, \frac{1}{2}), \ (\frac{5}{6}, 0, \frac{1}{6}), \ (\frac{2}{3}, \frac{1}{6}, \frac{1}{6}), \ (0, \frac{1}{2}, \frac{1}{2}), \ (\frac{1}{6}, \frac{2}{3}, \frac{1}{6}), \ (\frac{1}{6}, \frac{1}{6}, \frac{2}{3}), \ (\frac{1}{2}, \frac{1}{4}, \frac{1}{4}), \ (\frac{1}{4}, \frac{1}{2}, \frac{1}{4})$ and $(\frac{1}{4}, \frac{1}{4}, \frac{1}{2})$.

The coordinates of any point P (Fig. 2) within the element with respect to the global coordinate system are given by

$$x = L_1 x_1 + L_2 x_2 + L_3 x_3,$$
$$y = L_1 y_1 + L_2 y_2 + L_3 y_3, \tag{1}$$

where

$$L_i = A_i / A, \quad i = 1, 2, 3$$

and A is the area of the triangular element.

Again

$$1 = L_1 + L_2 + L_3. \tag{2}$$

From Eqs. (1) and (2) we get

$$L_i = (a_i + b_i x + c_i y)/2A, \quad i = 1, 2, 3,$$

where

$$A = \tfrac{1}{2}[(x_2 y_3 - x_3 y_2) + (x_3 y_1 - x_1 y_3) + (x_1 y_2 - x_2 y_1)],$$

$a_i = x_j y_k - x_k y_j, b_i = y_j - y_k$ and $c_i = x_k - x_j$ where the parameters i, j and k follow cyclic order of 1, 2 and 3.

The transverse displacement (w) and the rotations (θ_x and θ_y) of the normal are chosen as the complete fifth-order and fourth-order polynomials of area coordinates (L_1, L_2, L_3), respectively, and are expressed as follows:

$$w = [\overline{L0}]\{\alpha\}, \quad \theta_x = [\overline{L1}]\{\beta\} \quad \text{and} \quad \theta_y = [\overline{L1}]\{\gamma\}, \tag{3}$$

where

$$\begin{aligned}\{\overline{L0}\} = \{&L_1^5\ L_2^5\ L_3^5\ L_1^4L_2\ L_1L_2^4\ L_2^4L_3\ L_2L_3^4\ L_3^4L_1\ L_3L_1^4\\ &L_1^3L_2^2\ L_1^2L_2^3\ L_2^3L_3^2\ L_2^2L_3^3\ L_3^3L_1^2\ L_3^2L_1^3\\ &L_1^3L_2L_3\ L_2^3L_3L_1\ L_3^3L_1L_2\ L_1^2L_2^2L_3\ L_2^2L_3^2L_1\ L_3^2L_1^2L_2\},\end{aligned}$$

$$\begin{aligned}\{\overline{L1}\} = \{&L_1^4\ L_2^4\ L_3^4\ L_1^3L_2\ L_1L_2^3\ L_2^3L_3\ L_2L_3^3\ L_3^3L_1\ L_3L_1^3\ L_1^2L_2^2\\ &L_2^2L_3^2\ L_3^2L_1^2\ L_1^2L_2L_3\ L_2^2L_3L_1\ L_3^2L_1L_2\},\end{aligned}$$

$$\begin{aligned}\{\alpha\}^{\mathrm{T}} = \{&\alpha_1\ \alpha_2\ \alpha_3\ \alpha_4\ \alpha_5\ \alpha_6\ \alpha_7\ \alpha_8\ \alpha_9\ \alpha_{10}\ \alpha_{11}\ \alpha_{12}\ \alpha_{13}\ \alpha_{14}\\ &\alpha_{15}\ \alpha_{16}\ \alpha_{17}\ \alpha_{18}\ \alpha_{19}\ \alpha_{21}\},\end{aligned}$$

$$\{\beta\}^{\mathrm{T}} = \{\beta_1\ \beta_2\ \beta_3\ \beta_4\ \beta_5\ \beta_6\ \beta_7\ \beta_8\ \beta_9\ \beta_{10}\ \beta_{11}\ \beta_{12}\ \beta_{13}\ \beta_{14}\ \beta_{15}\},$$

and

$$\{\gamma\}^{\mathrm{T}} = \{\gamma_1\ \gamma_2\ \gamma_3\ \gamma_4\ \gamma_5\ \gamma_6\ \gamma_7\ \gamma_8\ \gamma_9\ \gamma_{10}\ \gamma_{11}\ \gamma_{12}\ \gamma_{13}\ \gamma_{14}\ \gamma_{15}\}.$$

Putting the values of nodal transverse displacements (w), nodal normal rotations (θ_x and θ_y) and nodal area coordinates (L_1, L_2, L_3) in the above Eqs. (3) the values of α's, β's and γ's can be determined as follows:

$$\{\overline{w}\} = [\Xi]\{\alpha\}, \quad \{\overline{\theta_x}\} = [\Psi]\{\beta\} \quad \text{and} \quad \{\overline{\theta}_y\} = [\Psi]\{\gamma\},$$

or

$$\{\alpha\} = [\Xi]^{-1}\{\overline{w}\}, \quad \{\beta\} = [\Psi]^{-1}\{\overline{\theta_x}\} \quad \text{and} \quad \{\gamma\} = [\Psi]^{-1}\{\overline{\theta_y}\},$$

where

$$\{\overline{w}\}^{\mathrm{T}} = \{w_1\ w_2\ w_3\ w_5\ w_6\ w_7\ w_8\ w_9\ w_{11}\ w_{12}\ w_{13}\ w_{14}\ w_{15}\ w_{17}\ w_{18}\ w_{19}\ w_{20}\ w_{21}\ w_{22}\ w_{23}\ w_{24}\},$$

$$\{\overline{\theta}_x\}^{\mathrm{T}} = \{\theta_{x1}\ \theta_{x3}\ \theta_{x4}\ \theta_{x5}\ \theta_{x7}\ \theta_{x9}\ \theta_{x10}\ \theta_{x11}\ \theta_{x13}\ \theta_{x15}\ \theta_{x16}\ \theta_{x17}\ \theta_{x22}\ \theta_{x23}\ \theta_{x24}\},$$

$$\{\overline{\theta}_y\}^{\mathrm{T}} = \{\theta_{y1}\ \theta_{y3}\ \theta_{y4}\ \theta_{y5}\ \theta_{y7}\ \theta_{y9}\ \theta_{y10}\ \theta_{y11}\ \theta_{y13}\ \theta_{y15}\ \theta_{y16}\ \theta_{y17}\ \theta_{y22}\ \theta_{y23}\ \theta_{y24}\}$$

and hence, the field variables (w, θ_x and θ_y) can be expressed in the following manner:

$$w = [\overline{N}_w]\{\overline{w}\}, \quad \theta_x = [\overline{N}_\theta]\{\bar{\theta}_x\} \quad \text{and} \quad \theta_y = [\overline{N}_\theta]\{\overline{\theta}_y\}, \tag{4}$$

where

$$[\overline{N}_w] = [\overline{L0}][\Xi]^{-1} \quad \text{and} \quad [\overline{N}_\theta] = [\overline{L1}][\Psi]^{-1}, \tag{5}$$

where $[\Xi]^{-1}$ is a (21×21) matrix and $[\Psi]^{-1}$ is a (15×15) matrix.

Eqs. (4) can be expressed in matrix form as below

$$\begin{Bmatrix} w \\ \theta_x \\ \theta_y \end{Bmatrix} = \begin{bmatrix} \overline{N}_w & 0 & 0 \\ 0 & \overline{N}_\theta & 0 \\ 0 & 0 & \overline{N}_\theta \end{bmatrix} \begin{Bmatrix} \overline{w} \\ \overline{\theta}_x \\ \overline{\theta}_y \end{Bmatrix} = [\overline{N}]\{\delta\}, \tag{6}$$

where

$$\{\delta\}^{\mathrm{T}} = \{\overline{w}\ \overline{\theta}_x\ \overline{\theta}_y\}.$$

As rotations of the normal θ_x and θ_y are independent variables and they are not derivatives of w, the effect of shear deformation can be easily incorporated as

$$\begin{Bmatrix} \phi_x \\ \phi_y \end{Bmatrix} = \begin{Bmatrix} \theta_x - w_{,x} \\ \theta_y - w_{,y} \end{Bmatrix}, \tag{7}$$

where ϕ_x and ϕ_y are average shear strain over the entire plate thickness and θ_x and θ_y are the total rotations of the normal.

The generalized stress–strain relationship may be expressed as

$$\{\sigma\} = [C]\{\varepsilon\}. \tag{8}$$

In the above equation the generalized stress vector is

$$\{\sigma\}^{\mathrm{T}} = \{M_x\ M_y\ M_{xy}\ Q_x\ Q_y\}. \tag{9}$$

The generalized strain vector $\{\varepsilon\}$ in terms of displacement fields is

$$\{\varepsilon\} = \begin{Bmatrix} -\theta_{x,x} \\ -\theta_{y,y} \\ -(\theta_{x,y} + \theta_{y,x}) \\ w_{,x} - \theta_x \\ w_{,y} - \theta_y \end{Bmatrix} \tag{10}$$

and the rigidity matrix $[C]$ is given by

$$[C] = \begin{bmatrix} C_{11} & C_{12} & 0 & 0 & 0 \\ C_{12} & C_{22} & 0 & 0 & 0 \\ 0 & 0 & C_{33} & 0 & 0 \\ 0 & 0 & 0 & C_{44} & 0 \\ 0 & 0 & 0 & 0 & C_{55} \end{bmatrix}, \tag{11}$$

where for isotropic materials $C_{11} = Et^3/\{12(1-v^2)\}$, $C_{12} = vC_{11}$, $C_{22} = C_{11}$, $C_{33} = (1-v)C_{11}/2$, $C_{44} = Et/\{2k(1+v)\}$ and $C_{55} = C_{44}, k$ is the warping factor which is taken as 1.2, assuming parabolic transverse shear strain distribution.

The strain–displacement relationship may be expressed as follows:

$$\{\varepsilon\} = \begin{bmatrix} 0 & -\overline{N}_{\theta,x} & 0 \\ 0 & 0 & -\overline{N}_{\theta,y} \\ 0 & -\overline{N}_{\theta,y} & -\overline{N}_{\theta,x} \\ \overline{N}_{w,x} & -\overline{N}_{\theta} & 0 \\ \overline{N}_{w,y} & 0 & -\overline{N}_{\theta} \end{bmatrix} \{\delta\} \tag{12}$$

or $\{\varepsilon\} = [B]\{\delta\}$ where $[B]$ is a (5×51) matrix.

Derivatives of $\overline{N}_{\theta}$ and $\overline{N}_{w}$ with respect to the global coordinates can be presented in matrix form as

$$\overline{N}_{\theta,x} = \{\overline{L2}\}[\overline{Q_1}], \quad \overline{N}_{w,x} = \{\overline{L1}\}[\overline{Q_2}], \quad \overline{N}_{\theta,y} = \{\overline{L2}\}[\overline{Q_3}] \text{ and } \overline{N}_{w,y} = \{\overline{L1}\}[\overline{Q_4}],$$

where

$$\{\overline{L2}\} = \{L_1^3\ L_2^3\ L_3^3\ L_1^2L_2\ L_1L_2^2\ L_2^2L_3\ L_2L_3^2\ L_3^2L_1\ L_3L_1^2\ L_1L_2L_3\}.$$

The matrices $\overline{Q_1}$ and $\overline{Q_3}$ are of order of 10×15 and the matrices $\overline{Q_2}$ and $\overline{Q_4}$ are of order of 15×21.

The matrix $[B]$ can be written as

$$[B] = [\overline{F}][\overline{Q}],$$

where

$$[\overline{F}] = \begin{bmatrix} \overline{L2} & 0 & 0 & 0 & 0 \\ 0 & \overline{L2} & 0 & 0 & 0 \\ 0 & 0 & \overline{L2} & 0 & 0 \\ 0 & 0 & 0 & \overline{L1} & 0 \\ 0 & 0 & 0 & 0 & \overline{L1} \end{bmatrix} \tag{13}$$

and

$$[\overline{Q}] = \begin{bmatrix} 0 & -\overline{Q_3} & 0 \\ 0 & 0 & -\overline{Q_4} \\ 0 & -\overline{Q_4} & -\overline{Q_3} \\ \overline{Q_1} & -\overline{Q_5} & 0 \\ \overline{Q_2} & 0 & -\overline{Q_5} \end{bmatrix}, \tag{14}$$

where $\overline{Q_5}$ is equal to $[\Xi]^{-1}$.

Thus, the element stiffness matrix $[K]^e$ is given by

$$[K]^e = \int [B]^{\mathrm{T}}[C][B]\,\mathrm{d}A = [\overline{Q}]^{\mathrm{T}} \int [\overline{F}]^{\mathrm{T}}[C][\overline{F}]\,\mathrm{d}A[\overline{Q}]. \tag{15}$$

Eq. (15) can be depicted as

$$[K]^e = [\overline{Q}]^{\mathrm{T}} \begin{bmatrix} C_{11}\rho_1 & C_{12}\rho_1 & 0 & 0 & 0 \\ C_{12}\rho_1 & C_{22}\rho_1 & 0 & 0 & 0 \\ 0 & 0 & C_{33}\rho_1 & 0 & 0 \\ 0 & 0 & 0 & C_{44}\rho_2 & 0 \\ 0 & 0 & 0 & 0 & C_{55}\rho_2 \end{bmatrix} [\overline{Q}],$$

where

$$\rho_1 = \int \{\overline{L2}\}^{\mathrm{T}}\{\overline{L2}\}\,\mathrm{d}A \quad \text{and} \quad \rho_2 = \int \{\overline{L1}\}^{\mathrm{T}}\{\overline{L1}\}\,\mathrm{d}A.$$

Carrying out the integrations ρ_1 and ρ_2 can be evaluated explicitly.

Finally the element stiffness matrix has got the following form:

$$[K]^e = \left[\begin{array}{c|c|c} C_{44}\overline{Q_1}^{\mathrm{T}}\rho_2\overline{Q_1} + C_{55}\overline{Q_2}^{\mathrm{T}}\rho_2\overline{Q_2} & -C_{44}\overline{Q_1}^{\mathrm{T}}\rho_2\overline{Q_5} & -C_{55}\overline{Q_2}^{\mathrm{T}}\rho_2\overline{Q_5} \\ \hline -C_{44}\overline{Q_5}^{\mathrm{T}}\rho_2\overline{Q_1} & C_{11}\overline{Q_3}^{\mathrm{T}}\rho_1\overline{Q_3} + C_{33}\overline{Q_4}^{\mathrm{T}}\rho_1\overline{Q_4} + C_{44}\overline{Q_5}^{\mathrm{T}}\rho_2\overline{Q_5} & C_{12}\overline{Q_3}^{\mathrm{T}}\rho_1\overline{Q_4} + C_{33}\overline{Q_4}^{\mathrm{T}}\rho_1\overline{Q_3} \\ \hline -C_{55}\overline{Q_5}^{\mathrm{T}}\rho_2\overline{Q_2} & C_{12}\overline{Q_4}^{\mathrm{T}}\rho_1\overline{Q_3} + C_{33}\overline{Q_3}^{\mathrm{T}}\rho_1\overline{Q_4} & C_{22}\overline{Q_4}^{\mathrm{T}}\rho_1\overline{Q_4} + C_{33}\overline{Q_3}^{\mathrm{T}}\rho_1\overline{Q_3} + C_{55}\overline{Q_5}^{\mathrm{T}}\rho_2\overline{Q_5} \end{array}\right]. \tag{16}$$

In a similar manner the element consistent mass matrix of an element can be derived explicitly using the above shape functions and can be expressed as

$$[M]^e = \begin{bmatrix} \rho t \Xi^{-\mathrm{T}} \rho_3 \Xi & 0 & 0 \\ 0 & \dfrac{\rho t^3}{12} \Psi^{-\mathrm{T}} \rho_2 \Psi & 0 \\ 0 & 0 & \dfrac{\rho t^3}{12} \Psi^{-\mathrm{T}} \rho_2 \Psi \end{bmatrix}, \tag{17}$$

where $\rho_3 = \int \{\overline{L0}\}^{\mathrm{T}} \{\overline{L0}\} \, \mathrm{d}A$ which can also be determined explicitly by carrying out the integration.

Stiffness and mass matrices obtained from Eqs. (16) and (17), respectively, are of the order of 51×51. These matrices have been reduced to the required matrices ($[K]^{\mathrm{er}}$ and $[M]^{\mathrm{er}}$) of the order of 39×39 by applying the Guyan reduction scheme [25] for global assembly. The reduced element stiffness ($[K]^{\mathrm{er}}$) and element consistent mass ($[M]^{\mathrm{er}}$) matrices can be assembled into the following final form for free vibration:

$$[K] - \omega^2 [M] = 0. \tag{18}$$

The above equation has been solved by the simultaneous iterative technique of Corr and Jenning [26] after substitution of boundary conditions to get the first few frequencies for the lower modes of the plate.

3. Numerical examples

3.1. Patch test for constant bending moment, pure shear and twisting moment

For all the examples Poisson's ratio of the plate material is taken as 0.3 and the warping factor (k) is assumed to be 1.2. To show the convergence characteristics and robustness of the element

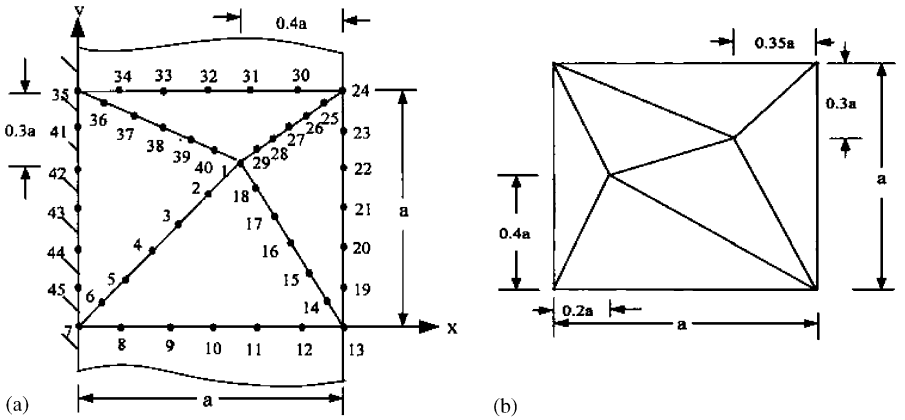

Fig. 3. Cantilever plate with edge loading.

developed in this paper a cantilever plate is considered (Fig. 3). The plate extends to infinity in the positive and negative y directions and is clamped along the edge $x = 0$, i.e., along the y-axis. The plate is subjected to a uniformly distributed constant moment M per unit length at the edge $x = a$. Two types of mesh geometries are solved for constant bending moment patch test. For the mesh geometry of Fig. 3(a), the boundary conditions are $w = 0$ at nodes 7,35,41,42,44 and 45, $\theta_x = 0$ at nodes 7,35,42,43 and 44 and $\theta_y = 0$ at nodes 7,9,10,11,13,20,21,22,24,31,32 33,35,42,43 and 44. The boundary conditions and constant moment condition are similarly assigned for the mesh geometry of Fig. 3(b). The non-dimensional transverse edge deflections (Et^3w/Ma^2) at the edge $x = a$ are numerically matching with the exact solutions (5.46000) for different thickness ratios ($t/h = 0.01, 0.1, 1.0, 10.0, 100.0$ and 1000.0) as expected. The same plate and the same mesh geometries are utilized for the shear patch test. In this case, a shear loading of V per unit length is applied on the edge $x = a$. Computed vertical displacements in non-dimensional form (Gtw/Va) at nodes 13, 19, 20, 22, 23 and 24 exactly agree with the elementary solutions including both shear and bending, and for shear only. The value of warping factor (k) is taken as unity for this example to correspond to the elementary solution and to simulate the effect of pure shear; the terms in the rigidity matrix corresponding to the bending stiffness are multiplied by a large quantity. For twisting patch test the plate geometry is shown in Fig. 4(a). Young's modulus of the plate material is taken as 10 000 psi and the plate thickness is 1 in. The plate is simply supported at points A, B and C ($w = 0$) and is subjected to a transverse load of 5 lb at D. The

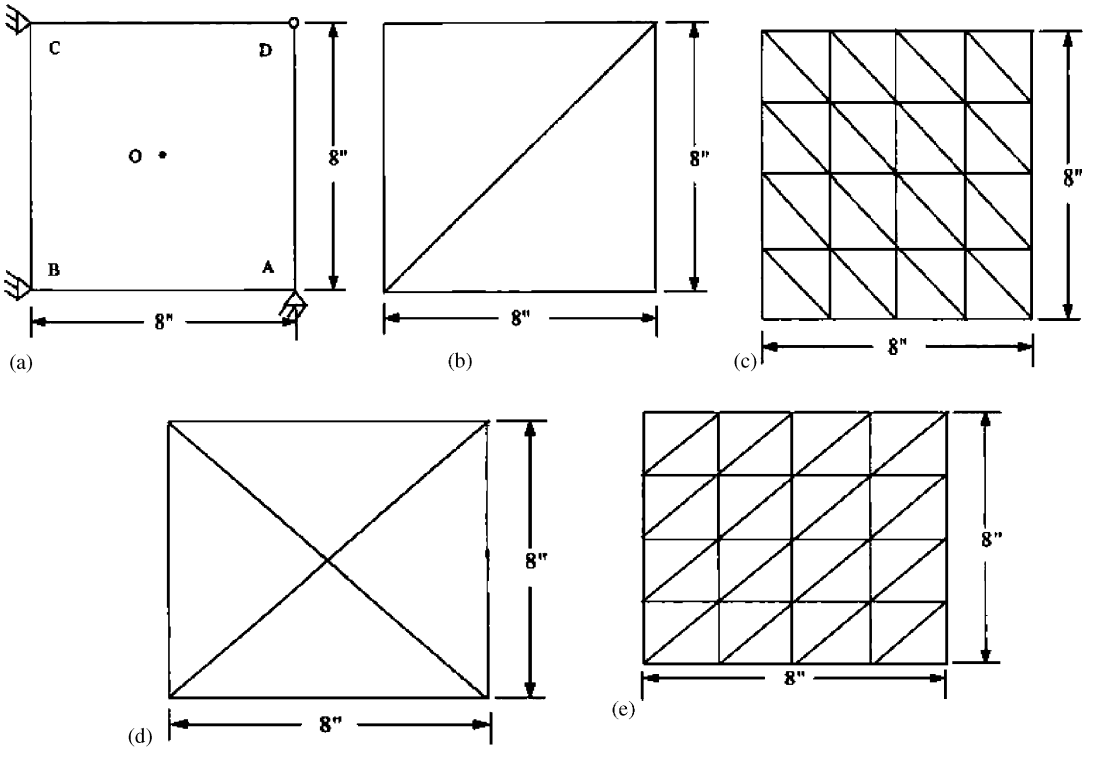

Fig. 4. Twisting of a square plate.

Table 1
Twisting patch test

Element type	Deflection (in)		M_x	M_y	M_{xy}
	Point D	Point O	(lb-in/in)	(lb-in/in)	(lb-in/in)
Fig. 3(a)	0.024960	0.06240[a]	0[b]	0[b]	2.50000
Fig. 3(b)	0.024960	0.06240[a]	0[b]	0[b]	2.50000
Fig. 4(b)	0.024960	0.06240[a]	0[b]	0[b]	2.50000
Fig. 4(c)	0.024960	0.06240	0[b]	0[b]	2.50000
Fig. 4(d)	0.024961	0.06240	0[b]	0[b]	2.50000
Fig. 4(e)	0.024960	0.06240	0[b]	0[b]	2.50000
DKT[c]—Fig.4(c)	0.024960	0.06240	0	0	2.50000
HSM[c]—Fig. 4(c)	0.024960	0.06240	0	0	2.50000
ACM[d]—Mesh 8 × 8	0.024972	0.06244	—	—	—
HCT[d]—Mesh 8 × 8	0.025002	0.06254	—	—	—
Thin plate theory	0.24960	0.06240	0	0	2.50000

[a]Interpolated values of the central deflections (Point O).
[b]Zero up to 4 significant digits after decimal point.
[c]Batoz et al. [27].
[d]Clough and Tocher [28].

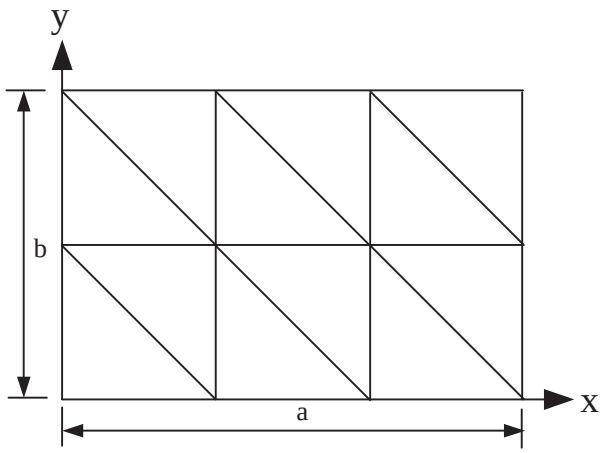

Fig. 5. Rectangular plate (Mesh 3 × 2).

terms C_{44} and C_{55} in the rigidity matrix are multiplied by a large number (10^6). The plate is solved for the mesh divisions as shown in Figs. 3(a), 3(b), 4(b), 4(c), 4(d) and 4(e). The deflections at point O and D and the moments are compared with thin plate solutions and other available published results (Table 1).

Table 2
Frequency parameters [$\lambda = (\omega b^2/\pi^2)\sqrt{(\rho t/D)}$] for square plates

Boundary condition	t/b	Source	Mode sequences					
			1	2	3	4	5	6
SSSS	0.001	PS-2	2.000	5.009	5.012	8.190	10.072	10.129
		PS-4	2.000	5.000	5.000	8.001	10.001	10.001
		PS-6	2.000	5.000	5.000	8.000	10.000	10.000
		PS-8[a]	2.000	5.000	5.000	8.000	10.000	10.000
		PS-8[b]	2.000	5.000	5.000	8.000	10.000	10.000
		[12]	2.000	5.000	5.000	8.000	10.000	10.000
		[29]	2.000	5.000	5.000	8.000	10.000	10.000
	0.20	PS-4	1.770	3.891	3.891	5.663	6.724	6.724
		PS-6	1.769	3.877	3.877	5.622	6.656	6.656
		PS-8	1.769	3.872	3.872	5.607	6.632	6.632
		PS-10	1.768	3.870	3.870	5.600	6.621	6.621
		PS-12	1.768	3.868	3.868	5.596	6.615	6.615
		PS-14[a]	1.768	3.868	3.868	5.594	6.611	6.611
		PS-14[b]	1.807	4.000	4.000	5.807	6.867	6.867
		[29]	1.768	3.866	3.866	5.588	6.601	6.601
		[30]	1.768	3.876	3.876	5.600	6.683	—
CCCC	0.001	PS-2	3.696	7.541	7.712	12.756	13.813	14.238
		PS-4	3.647	7.438	7.444	10.993	13.346	13.427
		PS-6	3.646	7.436	7.436	10.966	13.332	13.397
		PS-8[a]	3.646	7.436	7.436	10.965	13.332	13.395
		PS-8[b]	3.646	7.436	7.436	10.965	13.332	13.395
		[12]	3.647	7.438	7.438	10.970	13.338	13.339
		[29]	3.646	7.436	7.436	10.965	13.332	13.395
	0.20	PS-4	2.696	4.736	4.736	6.406	7.332	7.438
		PS-6	2.691	4.711	4.711	6.347	7.248	7.350
		PS-8	2.690	4.702	4.702	6.326	7.217	7.318
		PS-10	2.689	4.698	4.698	6.316	7.203	7.303
		PS-12	2.688	4.696	4.696	6.311	7.195	7.295
		PS-14[a]	2.688	4.694	4.694	6.308	7.190	7.290
		PS-14[b]	2.726	4.808	4.808	6.488	7.425	7.496
		[29]	2.688	4.691	4.691	6.299	7.177	7.276
		[30]	2.688	4.700	4.700	6.310	7.232	—
CSFF	0.001	PS-2	1.540	2.088	4.039	5.016	5.715	7.912
		PS-4	1.540	2.086	4.027	5.011	5.704	7.836
		PS-6	1.540	2.086	4.026	5.011	5.703	7.835
		PS-8[a]	1.539	2.086	4.026	5.010	5.702	7.834
		PS-8[b]	1.539	2.086	4.026	5.010	5.703	7.835
		[12]	1.549	2.095	4.030	5.040	5.737	7.839
		[29]	1.540	2.087	4.027	5.011	5.704	7.835
	0.20	PS-4	1.326	1.704	3.064	3.647	4.031	5.264
		PS-6	1.326	1.703	3.058	3.636	4.015	5.233
		PS-8	1.326	1.702	3.056	3.631	4.010	5.221
		PS-10	1.325	1.702	3.055	3.629	4.007	5.216

Table 2 (*continued*)

Boundary condition	t/b	Source	Mode sequences					
			1	2	3	4	5	6
		PS-12	1.325	1.702	3.054	3.628	4.006	5.213
		PS-14[a]	1.325	1.702	3.054	3.628	4.005	5.211
		PS-14[b]	1.342	1.749	3.241	3.729	4.156	5.512
		[29]	1.325	1.702	3.053	3.626	4.003	5.206

[a]Present study with rotary inertia with mesh division (8 × 8).
[b]Present study without rotary inertia.

Table 3
Frequency parameters $\lambda = (\omega b^2/\pi^2)\sqrt{(\rho t/D)}$ for rectangular plates: boundary conditions (SSSS)

a/b	t/b	Source	Mode sequences					
			1	2	3	4	5	6
1.0	0.001	PS-8	2.000	5.000	5.000	8.000	10.000	10.000
		[29]	2.000	5.000	5.000	8.000	10.000	10.000
	0.10	PS-14	1.932	4.609	4.609	7.075	8.622	8.622
		[24]	1.931	4.606	4.606	7.066	8.611	8.611
		[29]	1.932	4.608	4.608	7.072	8.616	8.616
	0.20	PS-14	1.768	3.868	3.868	5.594	6.611	6.611
		[24]	1.767	3.861	3.861	5.573	6.576	6.576
		[29]	1.768	3.866	3.866	5.588	6.601	6.601
1.5	0.001	PS-8	1.444	2.778	4.444	5.000	5.778	8.000
		[29]	1.445	2.778	4.445	5.000	5.778	8.000
	0.10	PS-14	1.408	2.649	4.131	4.610	5.267	7.076
		[29]	1.408	2.649	4.130	4.608	5.266	7.072
	0.20	PS-14	1.317	2.362	3.514	3.869	4.345	5.597
		[29]	1.316	2.361	3.512	3.866	4.341	5.588
2.0	0.001	PS-8	1.250	2.000	3.250	4.250	5.000	5.000
		[29]	1.250	2.000	3.250	4.250	5.000	5.000
	0.10	PS-14	1.223	1.932	3.077	3.962	4.610	4.610
		[29]	1.223	1.932	3.076	3.961	4.608	4.608
	0.20	PS-14	1.152	1.768	2.704	3.387	3.869	3.869
		[29]	1.152	1.768	2.702	3.385	3.866	3.866
2.5	0.001	PS-8	1.160	1.640	2.440	3.560	4.160	4.640
		[29]	1.160	1.640	2.440	3.560	4.160	4.640
	0.10	PS-14	1.136	1.594	2.340	3.354	3.884	4.301
		[29]	1.136	1.594	2.340	3.353	3.883	4.299
	0.20	PS-14	1.075	1.478	2.109	2.921	3.328	3.641
		[29]	1.075	1.478	2.109	2.919	3.325	3.638

Table 4
Frequency parameters $\lambda = (\omega b^2/\pi^2)\sqrt{(\rho t/D)}$ for rectangular plates: boundary conditions (SSCF)

a/b	t/b	Source	Mode sequences					
			1	2	3	4	5	6
1.0	0.001	PS-8	1.285	3.350	4.225	6.385	7.335	9.181
		[29]	1.285	3.350	4.225	6.385	7.335	9.181
	0.10	PS-14	1.241	3.081	3.915	5.656	6.358	7.961
		[29]	1.241	3.081	3.915	5.654	6.356	7.957
	0.20	PS-14	1.151	2.610	3.334	4.535	4.918	6.168
		[29]	1.151	2.610	3.333	4.532	4.914	6.160
1.5	0.001	PS-8	0.758	2.040	2.748	4.157	4.225	6.385
		[29]	0.758	2.040	2.748	4.157	4.225	6.385
	0.10	PS-14	0.736	1.950	2.556	3.781	3.915	5.656
		[29]	0.736	1.950	2.556	3.780	3.915	5.654
	0.20	PS-14	0.694	1.766	2.195	3.152	3.335	4.536
		[29]	0.694	1.766	2.195	3.151	3.333	4.532
2.0	0.001	PS-8	0.578	1.285	2.502	2.527	3.350	4.225
		[29]	0.578	1.286	2.502	2.527	3.350	4.225
	0.10	PS-14	0.563	1.241	2.365	2.377	3.081	3.915
		[29]	0.563	1.241	2.365	2.377	3.081	3.915
	0.20	PS-14	0.536	1.151	2.043	2.122	2.611	3.335
		[29]	0.536	1.151	2.042	2.121	2.610	3.333
2.5	0.001	PS-8	0.497	0.942	1.711	2.423	2.806	2.964
		[29]	0.497	0.942	1.711	2.423	2.806	2.964
	0.10	PS-14	0.485	0.913	1.643	2.275	2.654	2.745
		[29]	0.485	0.913	1.643	2.274	2.654	2.744
	0.20	PS-14	0.464	0.856	1.504	1.971	2.345	2.348
		[29]	0.464	0.856	1.503	1.970	2.344	2.348

3.2. Convergence study

For all the examples Poisson's ratio of the plate material is taken as 0.3 and the warping factor (k) is assumed to be 1.2. The geometry of the rectangular plate is shown in Fig. 5. The boundary conditions of the plate with clamped edge ($x = 0$), simply supported edge ($x = a$), clamped edge ($y = 0$) and free edge ($y = b$) are symbolized as CSCF. The eigenvalues obtained in the present investigation have been expressed in the non-dimensional form which is defined by the parameters $\lambda_i = (\omega_i b^2/\pi^2)\sqrt{(\rho t/D)}$. Several case studies have been investigated for isotropic rectangular plates with different thickness ratios ($t/b = 0.001$, 0.1 and 0.2), different aspect ratios ($a/b = 0.4, 0.6, 0.8, 1.0, 1.5, 2.0$ and 2.5) and 21 different combinations of simply supported (S), clamped (C) and free (F) boundary conditions.

Table 5
Frequency parameters, $\lambda = (\omega b^2/\pi^2)\sqrt{(\rho t/D)}$ for rectangular plates: boundary conditions (SSFF)

a/b	t/b	Source	Mode sequences					
			1	2	3	4	5	6
1.0	0.001	PS-8	0.976	1.635	3.721	3.946	4.735	7.167
		[24]	0.976	1.632	3.707	3.944	4.728	7.143
		[29]	0.977	1.636	3.722	3.946	4.736	7.167
	0.10	PS-14	0.957	1.559	3.431	3.684	4.337	6.299
		[24]	0.956	1.557	3.417	3.681	4.327	6.271
		[29]	0.957	1.559	3.431	3.684	4.336	6.297
	0.20	PS-14	0.910	1.428	2.953	3.169	3.645	5.026
		[24]	0.910	1.426	2.941	3.164	3.634	4.997
		[29]	0.910	1.428	2.952	3.168	3.644	5.022
1.5	0.001	PS-8	0.430	0.974	1.744	2.470	2.963	3.946
		[29]	0.433	0.975	1.744	2.470	2.963	3.946
	0.10	PS-14	0.426	0.934	1.687	2.332	2.780	3.684
		[29]	0.426	0.934	1.687	2.332	2.780	3.684
	0.20	PS-14	0.416	0.874	1.555	2.081	2.456	3.170
		[29]	0.416	0.874	1.555	2.081	2.455	3.168
2.0	0.001	PS-8	0.241	0.697	0.976	1.635	2.211	2.672
		[29]	0.244	0.698	0.977	1.635	2.211	2.672
	0.10	PS-14	0.240	0.670	0.957	1.559	2.122	2.531
		[29]	0.240	0.670	0.957	1.559	2.122	2.531
	0.20	PS-14	0.236	0.631	0.910	1.428	1.924	2.264
		[29]	0.236	0.631	0.910	1.428	1.924	2.263
2.5	0.001	PS-8	0.154	0.545	0.622	1.219	1.410	2.113
		[29]	0.160	0.547	0.624	1.220	1.411	2.114
	0.10	PS-14	0.153	0.524	0.614	1.168	1.371	2.005
		[29]	0.153	0.524	0.614	1.168	1.371	2.005
	0.20	PS-14	0.152	0.496	0.593	1.084	1.281	1.809
		[29]	0.152	0.496	0.593	1.084	1.281	1.808

Convergence studies have been carried out for three selected square plates. The plates are analyzed with and without the rotary inertia. The first one is with all edges simply supported (SSSS), the second one with all edges clamped (CCCC) and the third one with one edge ($x = 0$) clamped, one edge ($x = a$) simply supported and the remaining two edges free (CSFF). The non-dimensional frequency parameters (λ_i) for the first six modes are displayed with the available published results of Leissa [12], Liew et al. [29] and Kanaka Raju and Hinton [30] for thickness ratios (t/b) of 0.001 and 0.2 in Table 2. It has been found from tables that the rotary inertia has an almost null effect on the frequency response of thin plates ($t/b = 0.001$) but a great influence on the aforementioned response when the plates become thick ($t/b = 0.2$). For simply supported

Table 6
Frequency parameters, $\lambda = (\omega b^2/\pi^2)\sqrt{(\rho t/D)}$ for rectangular plates: boundary conditions (CCCC)

a/b	t/b	Source	Mode sequences					
			1	2	3	4	5	6
1.0	0.001	PS-8	3.646	7.436	7.436	10.965	13.332	13.395
		[29]	3.646	7.436	7.436	10.965	13.332	13.395
	0.10	PS-14	3.296	6.288	6.288	8.816	10.389	10.488
		[24]	3.294	6.277	6.277	8.786	10.340	10.438
		[29]	3.295	6.286	6.286	8.810	10.379	10.478
	0.20	PS-14	2.688	4.694	4.694	6.308	7.190	7.290
		[29]	2.688	4.691	4.691	6.299	7.177	7.276
1.5	0.001	PS-8	2.736	4.225	6.700	6.740	8.086	10.215
		[29]	2.736	4.226	6.700	6.740	8.086	10.214
	0.10	PS-14	2.525	3.798	5.739	5.831	6.793	8.432
		[29]	2.525	3.798	5.737	5.828	6.789	8.425
	0.20	PS-14	2.120	3.074	4.326	4.484	5.053	6.160
		[29]	2.120	3.073	4.322	4.480	5.046	6.148
2.0	0.001	PS-8	2.490	3.225	4.536	6.417	6.483	7.202
		[29]	2.491	3.225	4.536	6.417	6.483	7.202
	0.10	PS-14	2.309	2.952	4.072	5.573	5.609	6.129
		[29]	2.309	2.952	4.071	5.571	5.607	6.126
	0.20	PS-14	1.950	2.453	3.292	4.209	4.376	4.604
		[29]	1.950	2.452	3.290	4.205	4.371	4.598
2.5	0.001	PS-8	2.396	2.818	3.589	4.729	6.232	6.392
		[29]	2.396	2.818	3.589	4.729	6.233	6.392
	0.10	PS-14	2.226	2.597	3.270	4.243	5.479	5.503
		[29]	2.226	2.597	3.270	4.242	5.476	5.500
	0.20	PS-14	1.883	2.178	2.703	3.431	4.159	4.310
		[29]	1.883	2.177	2.702	3.428	4.154	4.305

square plates the maximum deviation of the nondimensional frequency parameters by the present analysis with and without rotary inertia from those obtained by Liew et al. [29] is 0.15% and 4.03%, respectively. As the present element (with rotary inertia) predicts the frequency parameters more accurately, all the plates are analyzed considering the rotary inertia. From Table 2 it is found that the present element has good convergence characteristics and good accuracy to predict the frequency parameters for thin plates ($t/b = 0.001$) as well as thick plates ($t/b = 0.2$). It is also observed that the frequency parameters (λ_i) monotonically decrease and approach the exact values with the increase in the number of elements used.

3.3. Parametric study

To study the effect of boundary conditions, thickness ratios and aspect ratios, 21 different boundary conditions with three different thickness ratios ($t/b = 0.001, 0.1$ and 0.2) and seven

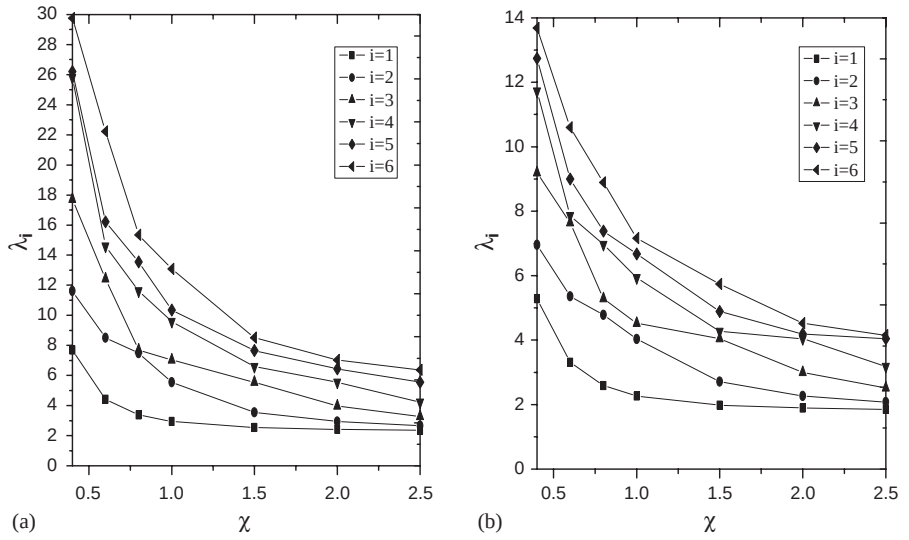

Fig. 6. First six nondimensional frequency parameters (λ_i) of SSCC Mindlin plates with respect to aspect ratio (χ). (a) $t/b = 0.001$, (b) $t/b = 0.2$.

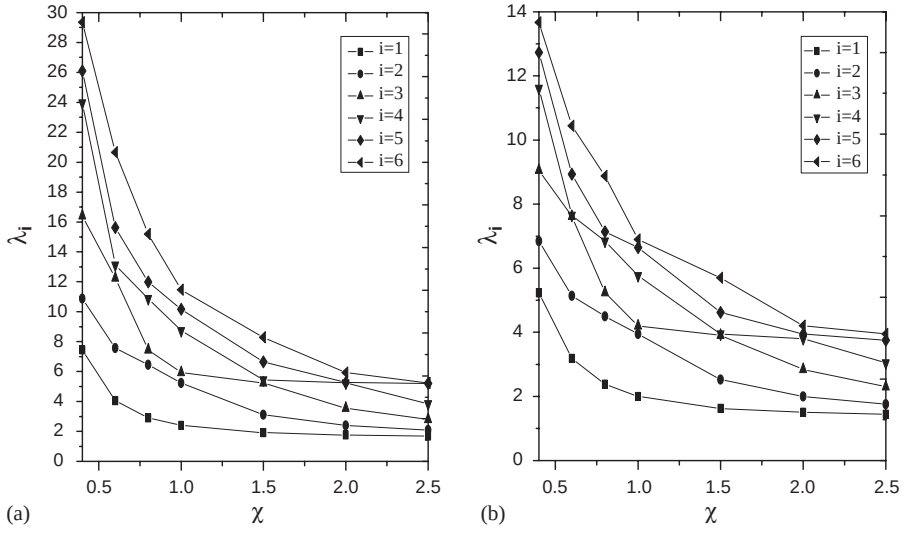

Fig. 7. First six nondimensional frequency parameters (λ_i) of SSCS Mindlin plates with respect to aspect ratio (χ). (a) $t/b = 0.001$, (b) $t/b = 0.2$.

different aspect ratios (a/b) have been considered in the present investigation. The numerical data for four different aspect ratios ($a/b = 1.0, 1.5, 2.0$ and 2.5) from the present formulation have been given in Tables 3–6 along with the published results of Liessa [12], Sheikh et al. [24] and Liew et al. [29] for five different boundary conditions (SSSS, SSCF, SSFF and CCCC). From the tables it can

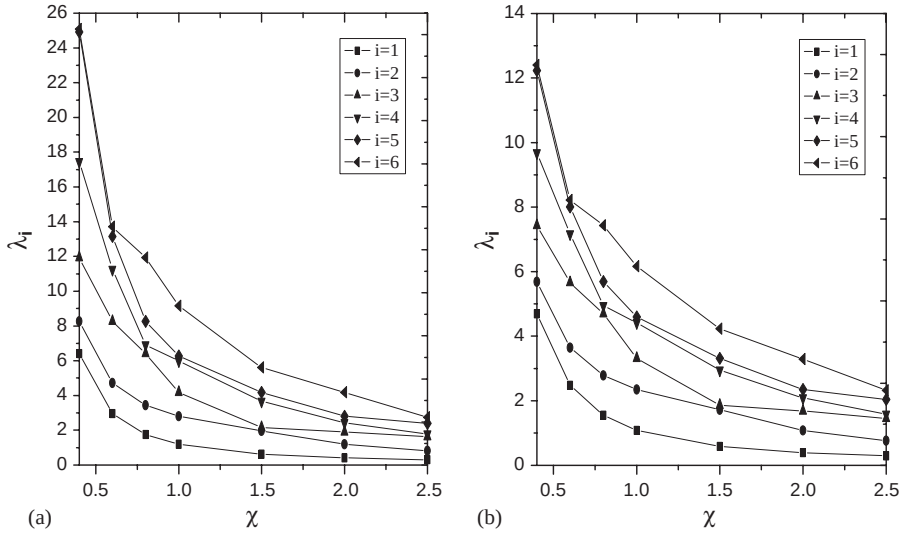

Fig. 8. First six nondimensional frequency parameters (λ_i) of SSSF Mindlin plates with respect to aspect ratio (χ). (a) $t/b = 0.001$, (b) $t/b = 0.2$.

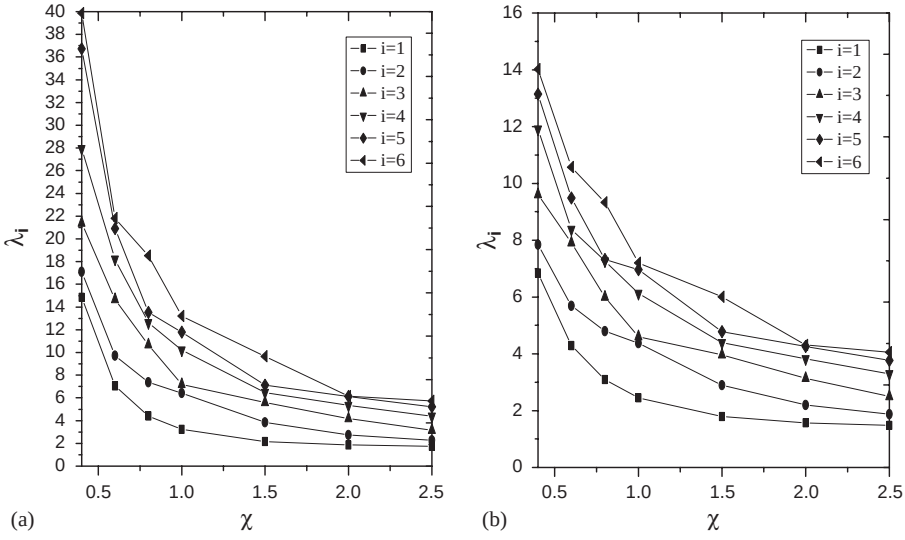

Fig. 9. First six nondimensional frequency parameters (λ_i) of CCCS Mindlin plates with respect to aspect ratio (χ). (a) $t/b = 0.001$, (b) $t/b = 0.2$.

be seen that the aspect ratios, thickness ratios and boundary conditions have great influences on the normal modes of vibration of rectangular plates. It is also found that as the thickness of the plate increases the frequency parameter decreases clearly showing the effect of rotary inertia and shear deformation on free vibration of plates. It is further observed that the frequency parameters

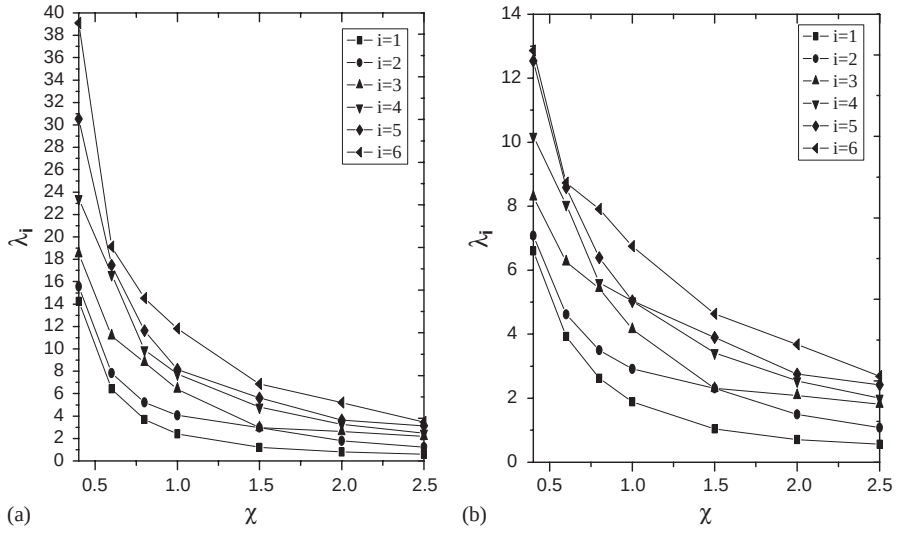

Fig. 10. First six nondimensional frequency parameters (λ_i) of CCCF Mindlin plates with respect to aspect ratio (χ). (a) $t/b = 0.001$, (b) $t/b = 0.2$.

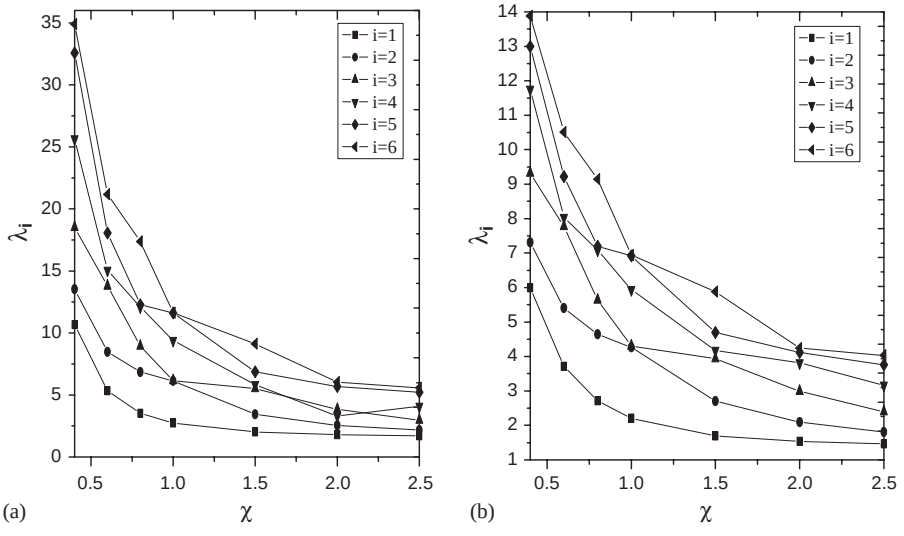

Fig. 11. First six nondimensional frequency parameters (λ_i) of CSCS Mindlin plates with respect to aspect ratio (χ). (a) $t/b = 0.001$, (b) $t/b = 0.2$.

for simply supported rectangular plates are much lower than those for clamped rectangular plates. This implies that higher constraints on the edges increases the flexural rigidity of the plate and results in higher frequency response. Liew et al. [29] analyzed the problems using Rayleigh–Ritz procedure considering Mindlin's plate theory. From the results it is found that higher mesh

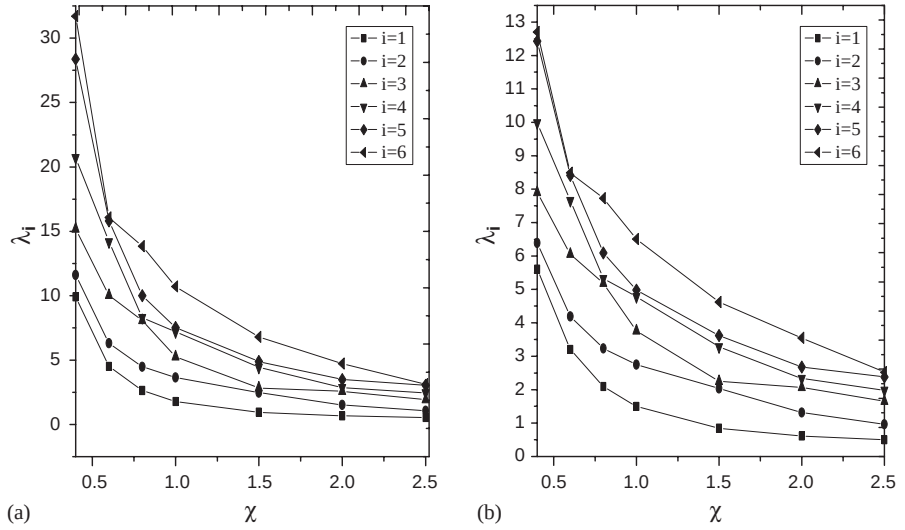

Fig. 12. First six nondimensional frequency parameters (λ_i) of CSCF Mindlin plates with respect to aspect ratio (χ). (a) $t/b = 0.001$, (b) $t/b = 0.2$.

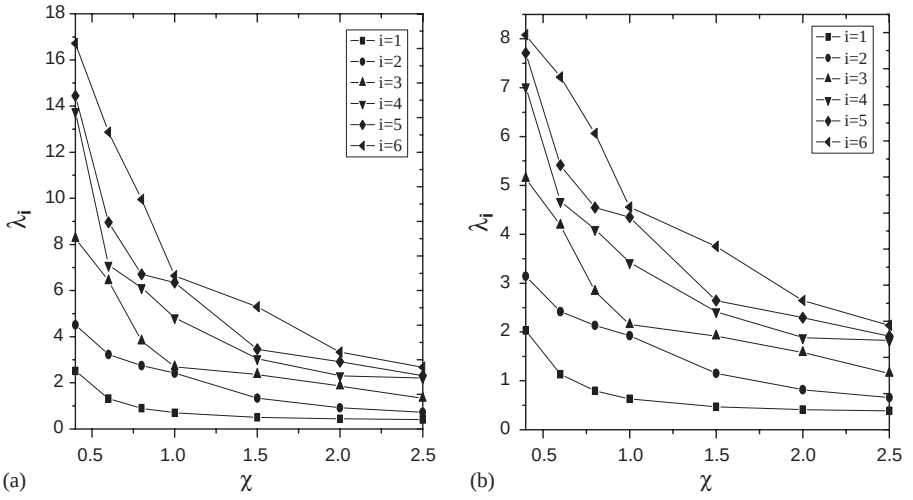

Fig. 13. First six nondimensional frequency parameters (λ_i) of CFCF Mindlin plates with respect to aspect ratio (χ). (a) $t/b = 0.001$, (b) $t/b = 0.2$.

divisions are required to get the converged results for thick ($t/a = 0.1$ and 0.2) plates in comparison with the thin ($t/a = 0.001$) plates. The results obtained from the present analysis are given in graphical form in Figs. 6–22 for the remaining boundary conditions (SSCC, SSCS, SSSF, CCCS, CCCF, CSCS, CSCF, CFCF, CCSF, CSSF, CFSF, CCFF, CSFF, CFFF, SFSF, SFFF and FFFF). The first six non-dimensional frequency parameters are plotted as a function of

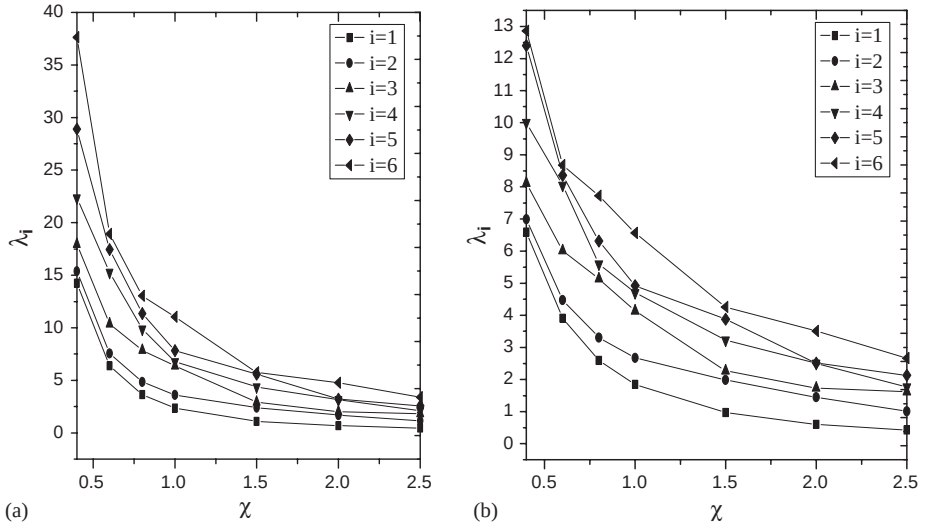

Fig. 14. First six nondimensional frequency parameters (λ_i) of CCSF Mindlin plates with respect to aspect ratio (χ). (a) $t/b = 0.001$, (b) $t/b = 0.2$.

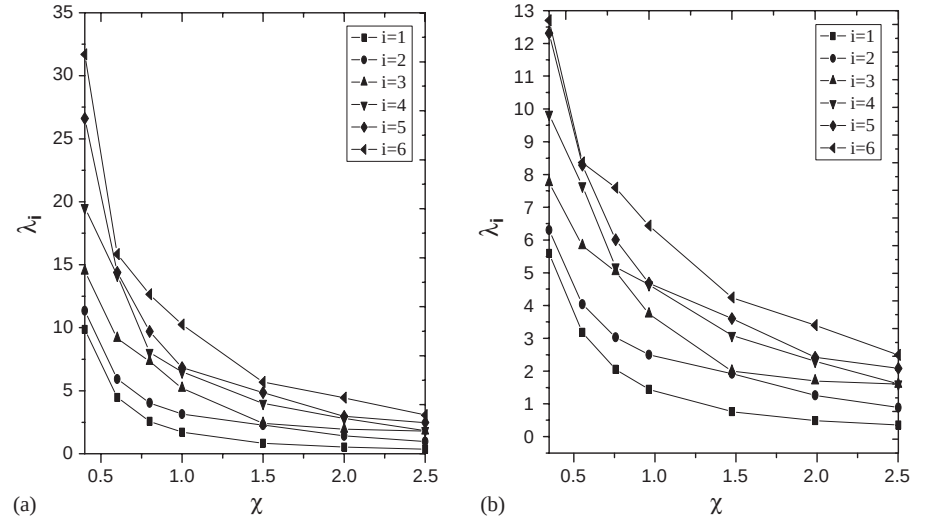

Fig. 15. First six nondimensional frequency parameters (λ_i) of CSSF Mindlin plates with respect to aspect ratio (χ). (a) $t/b = 0.001$, (b) $t/b = 0.2$.

aspect ratio (a/b) for two different thickness ratios ($t/b = 0.001$ and 0.2) in sub-plots (a) and (b) in each figure. From these figures it is observed that the frequency parameters decrease as the aspect ratio increases.

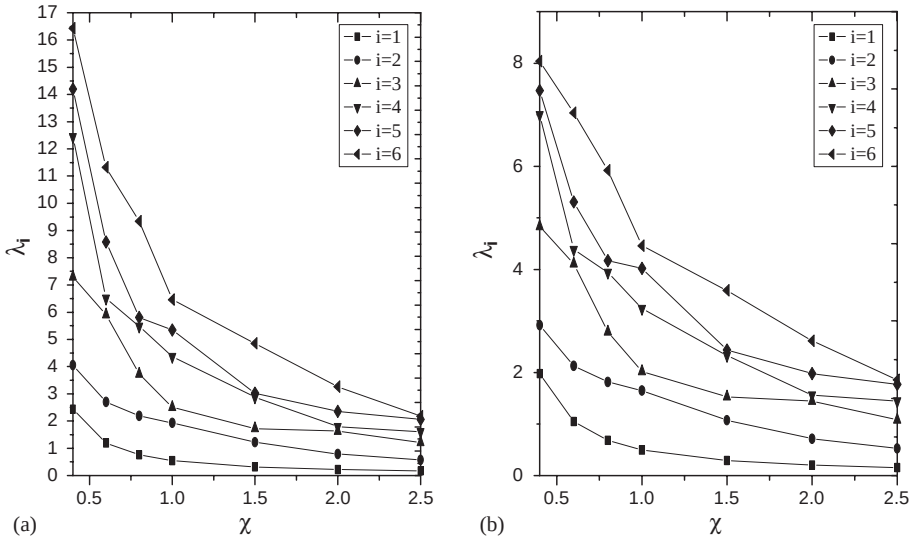

Fig. 16. First six nondimensional frequency parameters (λ_i) of CFSF Mindlin plates with respect to aspect ratio (χ). (a) $t/b = 0.001$, (b) $t/b = 0.2$.

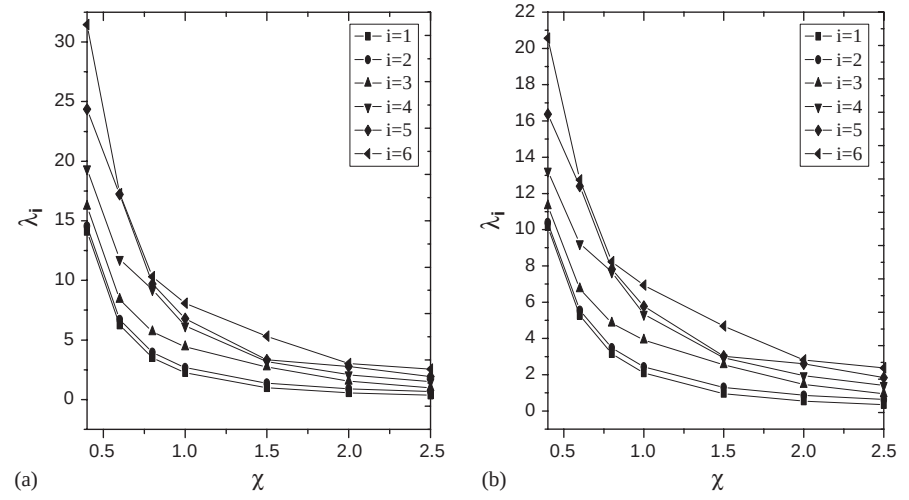

Fig. 17. First six nondimensional frequency parameters (λ_i) of CCFF Mindlin plates with respect to aspect ratio (χ). (a) $t/b = 0.001$, (b) $t/b = 0.2$.

4. Conclusions

A 24 node triangular plate bending element with 51 degrees of freedom has been utilized to investigate the free vibration of isotropic rectangular plates with different thickness ratios, aspect

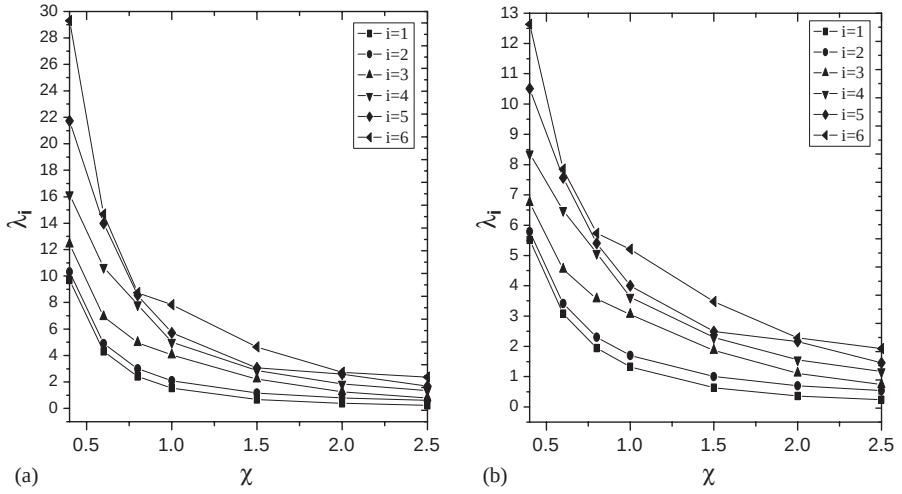

Fig. 18. First six nondimensional frequency parameters (λ_i) of CSFF Mindlin plates with respect to aspect ratio (χ). (a) $t/b = 0.001$, (b) $t/b = 0.2$.

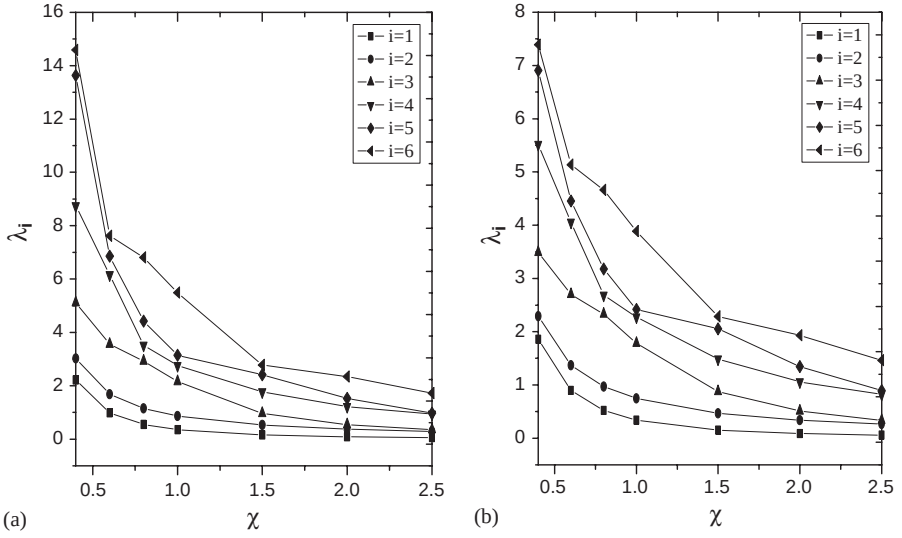

Fig. 19. First six nondimensional frequency parameters (λ_i) of CFFF Mindlin plates with respect to aspect ratio (χ). (a) $t/b = 0.001$, (b) $t/b = 0.2$.

ratios and boundary conditions. The degrees of freedom associated with the six internal nodes are condensed by the Guyan reduction scheme to get the reduced element stiffness and mass matrices of the order of 39×39. A comparative study of present results with those of earlier investigators

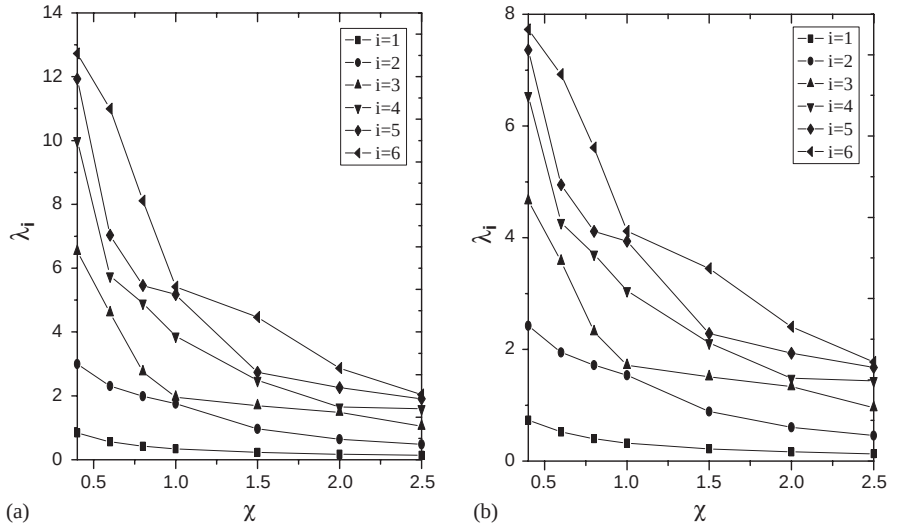

Fig. 20. First six nondimensional frequency parameters (λ_i) of SFSF Mindlin plates with respect to aspect ratio (χ). (a) $t/b = 0.001$. (b) $t/b = 0.2$.

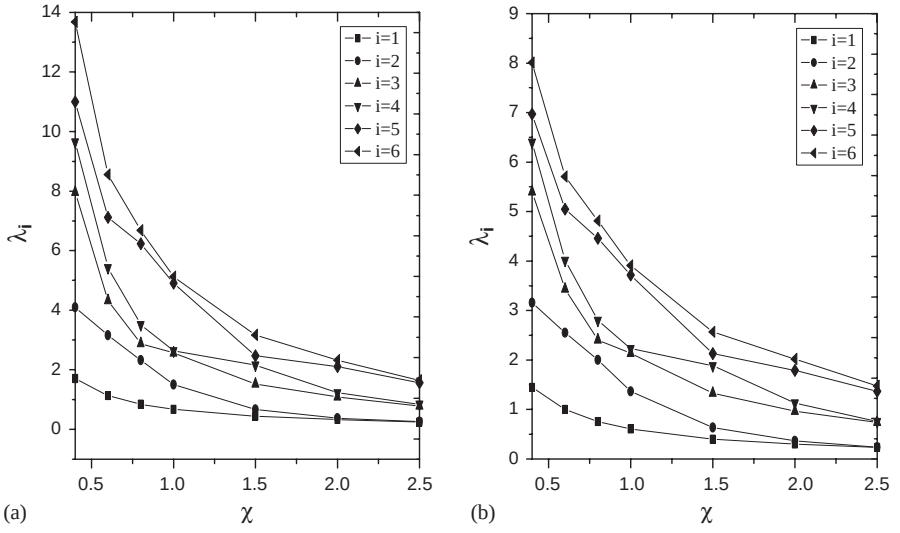

Fig. 21. First six nondimensional frequency parameters (λ_i) of SFFF Mindlin plates with respect to aspect ratio (χ). (a) $t/b = 0.001$, (b) $t/b = 0.2$.

shows the rapid convergence characteristics and accuracy of the present element for very thin to thick plates. It can also be concluded that due to increase of node numbers on the edges of the proposed element the mass and rotary inertia distribution at different nodes are such that the

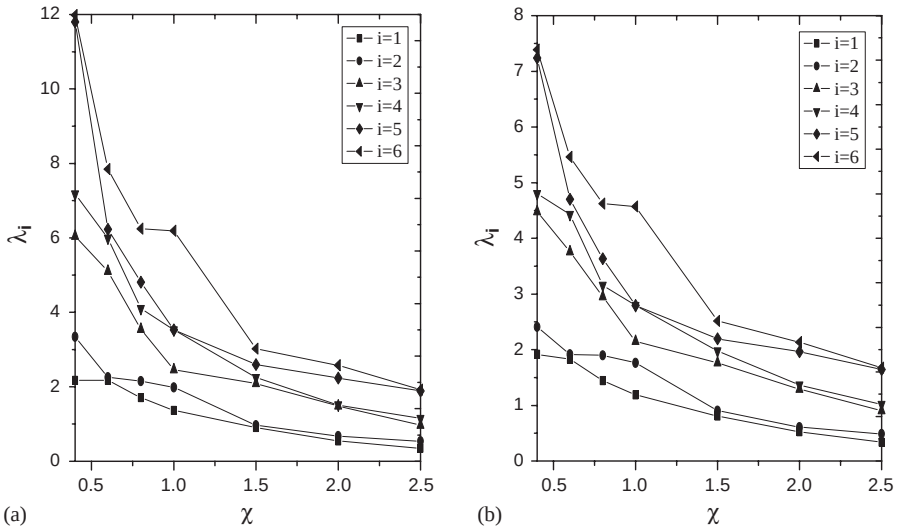

Fig. 22. First six nondimensional frequency parameters (λ_i) of FFFF Mindlin plates with respect to aspect ratio (χ). (a) $t/b = 0.001$, (b) $t/b = 0.2$.

mass as well as rotary inertia associated with the internal nodes are negligible compared to those with the nodes on the edges. This helps the application of the Guyan reduction scheme to this element efficiently and accurately.

References

[1] O.C. Zienkiewicz, R.L. Taylor, *The Finite Element Methods (Two Volumes)*, McGraw Hill, New York, 1988.
[2] R.D. Cook, D.S. Malkus, M.E. Plesha, *Concepts and Applications of Finite Element Analysis*, Wiley, New York, 1989.
[3] A.W. Liessa, *Vibration of Plates (NASA SP-160)*, US Government Printing Office, Washington, DC, 1969.
[4] A.W. Liessa, Recent research in plate vibrations, 1973–1976: classical theory, *The Shock and Vibration Digest* 9 (10) (1977) 13–24.
[5] A.W. Liessa, Recent research in plate vibrations, 1973–1976: complicating effects, *The Shock and Vibration Digest* 9 (11) (1977) 21–35.
[6] A.W. Liessa, Plate vibration research, 1976–1980: classical theory, *The Shock and Vibration Digest* 13 (9) (1981) 11–22.
[7] A.W. Liessa, Plate vibration research, 1976–1980: complicating effects, *The Shock and Vibration Digest* 13 (10) (1981) 19–36.
[8] A.W. Liessa, Plate vibration research,1981–1985—part I: classical theory, *The Shock and Vibration Digest* 19 (2) (1987) 11–18.
[9] A.W. Liessa, Plate vibration research, 1981–1985—part II: complicating effects, *The Shock and Vibration Digest* 19 (3) (1987) 10–24.
[10] K.M. Liew, Y. Xiang, S. Kitipornchai, Research on thick plate vibration: a literature survey, *Journal of Sound and Vibration* 180 (1) (1995) 163–176.
[11] G.Y. Yamada, T. Irie, Plate vibration research in Japan, *Applied Mechanics Reviews* 40 (1987) 879–892.
[12] A.W. Liessa, The free vibration of rectangular plates, *Journal of Sound and Vibration* 31 (1973) 257–293.

[13] K.M. Liew, K.Y. Lam, S.T. Chow, Free vibration analysis of rectangular plates using orthogonal plate function, *Computers & Structures* 34 (1990) 79–85.
[14] S.M. Dickinson, A.D. Blasio, On the use of orthogonal polynomials in the Rayleigh–Ritz method for the study of the flexural vibration and buckling of isotropic and orthotropic rectangular plates, *Journal of Sound and Vibration* 108 (1986) 51–62.
[15] S.P. Lim, K.H. Lee, N.R. Senthilnathan, Rayleigh–Ritz vibration analysis of thick plates using a simple higher order theory, *Journal of Sound and Vibration* 130 (1989) 163–166.
[16] Y.K. Cheung, D. Zhou, Vibrations of moderately thick rectangular plates in terms of a set of static Timoshenko beam functions, *Computers & Structures* 78 (2000) 757–768.
[17] D. Zhou, Y.K. Cheung, F.T.K. Au, S.H. Lo, Three-dimensional vibration analysis of thick rectangular plates using Chebyshev polynomial and Ritz method, *International Journal of Solids and Structures* 39 (2002) 6339–6353.
[18] M.M. Hrabok, T.M. Hrudey, A review and catalogue of plate bending finite elements, *Computers & Structures* 19 (3) (1984) 479–495.
[19] J. Petrolito, A modified ACM element for thick plate analysis, *Computers & Structures* 32 (1989) 1303–1309.
[20] F.G. Yuan, R.E. Miller, A cubic triangular finite element for flat plates with shear, *International Journal for Numerical Methods in Engineering* 28 (1989) 109–126.
[21] D. Sengupta, Stress analysis of flat plates with shear using explicit stiffness method, *International Journal for Numerical Methods in Engineering* 32 (1991) 1289–1409.
[22] J.L. Batoz, I. Katili, On a simple triangular Reissner/Mindlin plate element based on incompatible modes and discrete constraints, *International Journal for Numerical Methods in Engineering* 35 (1992) 1603–1632.
[23] Xu. Zhongnian, A thick–thin triangular plate element, *International Journal for Numerical Methods in Engineering* 33 (1992) 963–973.
[24] A.H. Sheikh, S. Haldar, D. Sengupta, Vibration of plates in different situations using a high-precision shear deformable element, *Journal of Sound and Vibration* 253 (2002) 329–345.
[25] R.J. Guyan, Reduction of stiffness and mass matrices, *AIAA Journal* 3 (2) (1965) 380.
[26] R.B. Corr, A. Jennings, A simultaneous iteration algorithm for symmetric eigenvalue problems, *International Journal for Numerical Methods in Engineering* 10 (1976) 647–663.
[27] J.L. Batoz, K.J. Bathe, L.W. Ho, A study of three-node triangular plate bending elements, *International Journal for Numerical Methods in Engineering* 15 (1980) 1771–1812.
[28] R.W. Clough, J.L. Tocher, Finite element stiffness matrices for analysis of plate bending, in: *Proceedings of the First Conference on Matrix Methods in Structural Mechanics:* Wright-Patterson Air Force Base, OH, 1965, pp. 515–545.
[29] K.M. Liew, Y. Xiang, S. Kitipornchai, Transverse vibration of thick rectangular plates—I. Comprehensive sets of boundary conditions, *Computers & Structures* 49 (1993) 1–29.
[30] K. Kanaka raju, E. Hinton, Natural frequencies and mode of rhombic Mindlin plates, *Earthquake Engineering Structures and Dynamics* 8 (1980) 55–62.